ORIGINAL ARTICLE

Locating wind farms by seismic interferometry and migration

**Tobias Friedrich · Toni Zieger ·
Thomas Forbriger · Joachim R. R. Ritter**

Abstract We present a case study on the detection and quantification of seismic signals induced by operating wind turbines (WTs). We spatially locate the sources of such signals in data which were recorded at 11 seismic stations in 2011 and 2012 during the TIMO project (Deep Structure of the Central Upper Rhine Graben). During this time period, four wind farms with altogether 12 WTs were in operation near the town of Landau, Southwest Germany. We locate WTs as sources of continuous seismic signals by application of seismic interferometry and migration of the energy found in cross-correlograms. A clear increase of emitted seismic energy with rotor speed confirms that the observed signal is induced by WTs. We can clearly distinguish wind farms consisting of different types of WTs (different hub height and rotor diameter) corresponding to different stable frequency bands (1.3–1.6 Hz, 1.75–1.95 Hz and 2.0–2.2 Hz) which do not depend on wind speed. The peak frequency apparently is controlled by the elastic eigenmodes of the structure rather than the passing of blades at the tower. From this we conclude that vibrations are coupled into the ground at the foundation and propagate as Rayleigh waves (and not as infrasound). The migration velocity of 320 m/s corresponds to their group velocity. The applied migration method can contribute to the assessment of local sources of seismic noise. This topic gets growing attention in the seismological community. In particular, the recent boost of newly installed wind farms is a threat to seismological observatories such as the Black Forest Observatory (BFO) and the Gräfenberg array (GRF) or gravitational wave observatories (e.g. LIGO, VIRGO) in terms of a sensitivity degradation of such observatories.

Keywords Seismology · Seismic noise ·
Wind turbines · Migration · Seismic interferometry ·
Cross-correlation

T. Friedrich · T. Zieger (✉) · T. Forbriger · J. R. R. Ritter
Karlsruhe Institute of Technology (KIT), Geophysical
Institute (GPI), Karlsruhe, Germany
e-mail: toni.zieger@kit.edu

1 Introduction

The influences of wind turbines (WTs) on local seismic stations, seismological observatories and gravitational wave observatories is becoming an important topic inside the seismological community, especially after the large increase of new installations of WTs to boost renewable energy all over the world. Several studies (e.g. Schofield 2001; Styles et al. 2005; Saccorotti et al. 2011; Xi Engineering Consultants Ltd. 2014; Stammler and Ceranna 2016; Flores Estrella et al. 2017; Zieger and Ritter 2017; Neuffer and Kremers 2017) investigate the seismic emissions of WTs. The majority of them focus on the increase of the seismic noise level going along with the installation of new WTs in the vicinity of the seismic stations. However,

the data analyses do not clearly identify the WTs as the cause of the increased seismic signal level by locating the sources of the observed seismic waves. In the present study we demonstrate how sources of continuous signals can be located by the migration approach of Horstmann and Forbriger (2010) and be identified as wind farms. After a slight modification this procedure enables us to investigate the characteristic increase of generated seismic energy with increasing wind speed for a single, selected wind farm in the presence of other sources.

An early, comprehensive study on WT-induced signals in seismic recordings was published by Styles et al. (2005). They identify the characteristic frequencies of the WTs such as the blade-passing frequency (three times the rotation frequency) and their multiples at the Eskdalemuir Array in Scotland, Great Britain. They assume seismic waves propagating as vertically polarised P-SV (Rayleigh) waves excited by the WTs and demonstrate an increase of the amplitude with increasing wind speed. Schofield (2001) suggests that the propagation of WT-induced signals is partly through infrasound with an attenuation factor proportional to $1/R$ (where R is the distance between WT and observation point) for seismic measurements at the Stateline Wind Project. Saccorotti et al. (2011) investigate the vibrations produced by a wind farm near the VIRGO Gravitational Wave Observatory in Italy and present a simple model of wave propagation: the combination of direct surface waves with dominating Love waves and body waves reflected at the boundary between marine, fluvial, and lacustrine sediments and the carbonate basement in approximately 800 m depth. Gassenmeier et al. (2015) developed a single-station approach to investigate the direction of the incoming seismic noise and identify emitted Rayleigh waves of a nearby wind farm. Stammler and Ceranna (2016) examine the influence of WTs on seismic recordings at the Gräfenberg Array (GRF). They demonstrate a decrease of the detection capability of the GRF stations in the frequency band of 1–7 Hz due to an increasing number of WTs with a dependence on wind speed of the levels of noise spectra of all stations. They also present signals emitted by WTs close to 1.15 Hz which are detectable at distances larger than 15 km to the nearest seismic station.

In the current study, we focus on WT-induced signals identified by Zieger and Ritter (2017) in the area around the town of Landau, Southwest Germany, and on locating their sources by application of seismic interferometry. We use the migration method (see Section 3) introduced by Horstmann and Forbriger (2010) for locating industrial noise sources in Bucharest, Romania. A very similar approach was applied by Mündel (2009) to locate WTs near Ketzin, Northeast Germany, and by others to locate sources of ocean microseisms (Shapiro et al. 2006; Zeng and Ni 2010) or source regions of seismic tremors in volcanic areas (e.g. Ballmer et al. 2013; Droznin et al. 2015). An advancement of this method is the so-called *double-correlation method* by Li et al. (2017), who use cross-correlations of cross-correlograms of two station pairs (three stations in total, one of these as a reference station). As a consequence, noise is suppressed in a superior way and the source region is focussed more distinctly. Sgattoni et al. (2017) use this method to locate tremor at the Katla volcano, Iceland.

2 Setting

The town of Landau is located in the southwestern part of Germany, about 30 km northwest of the city of Karlsruhe. The area is within the central Upper Rhine Graben with a ca. 300-m-thick layer of unconsolidated Cenozoic sediments at the surface. The region is of seismological interest because of the natural seismicity of the Upper Rhine Graben and because of induced seismicity at two geothermal power plants (Vasterling et al. 2017; Ritter 2011). Due to the seismic monitoring long-term broadband recordings of a dense seismic network are available. Data are provided by the "Erdbebendienst Südwest", the "Federal Institute for Geosciences and Natural Resources (BGR)", and the "Karlsruher Broadband Array (KABBA)". Several WTs are located in the vicinity of the seismic network which went into production of electrical power at different times. Table 1 gives an overview of the WTs in operation during 2011 and 2012. The exact locations of these WTs are shown in Fig. 1. With overall four wind farms and a dense seismic network, the area around Landau is well suited for the current study. As shown in Table 1, the first WTs were installed in September 2004. Seismic data are not available for times before December 2004. Hence, we are unable to analyse seismic signals without influences of WTs.

Table 1 List of the WTs near Landau (Fig. 1) which were in operation during 2011 and 2012

Wind farm	Commissioning	WT type	P in MW	d in m	h in m
Bellheim	27-09–2004	GE Wind Energy 1.5sl	1.5	77	100
Bellheim	27-09–2004	GE Wind Energy 1.5sl	1.5	77	100
Bellheim	27-09–2004	GE Wind Energy 1.5sl	1.5	77	100
Rülzheim	18-05–2005	Fuhrländer FL MD77	1.5	77	100
Rülzheim	18-05–2005	Fuhrländer FL MD77	1.5	77	100
Rülzheim	23-03–2006	Fuhrländer FL MD77	1.5	77	100
Herxheimweyher	28-09–2005	Fuhrländer FL MD77	1.5	77	100
Herxheimweyher	30-09–2005	Fuhrländer FL MD77	1.5	77	100
Herxheimweyher	10-10–2005	Fuhrländer FL MD77	1.5	77	100
Offenbach	22-02–2008	Vestas V90	2.0	90	105
Offenbach	22-02–2008	Vestas V90	2.0	90	105
Offenbach	22-02–2008	Vestas V90	2.0	90	105

Specified are date of commissioning, the WT type, the nominal electric power P, the rotor diameter d and the hub height h of the turbines. The WTs of GE and Fuhrländer have the same technical specifications. The WTs of the type Vestas V90 have a larger rotor diameter, larger hub height and more power (http://www.energieatlas.rlp.de/earp/daten/ee-anlagen/, de.wikipedia.org/wiki/Liste_von_Windkraftanlagen_in_Rheinland-Pfalz)
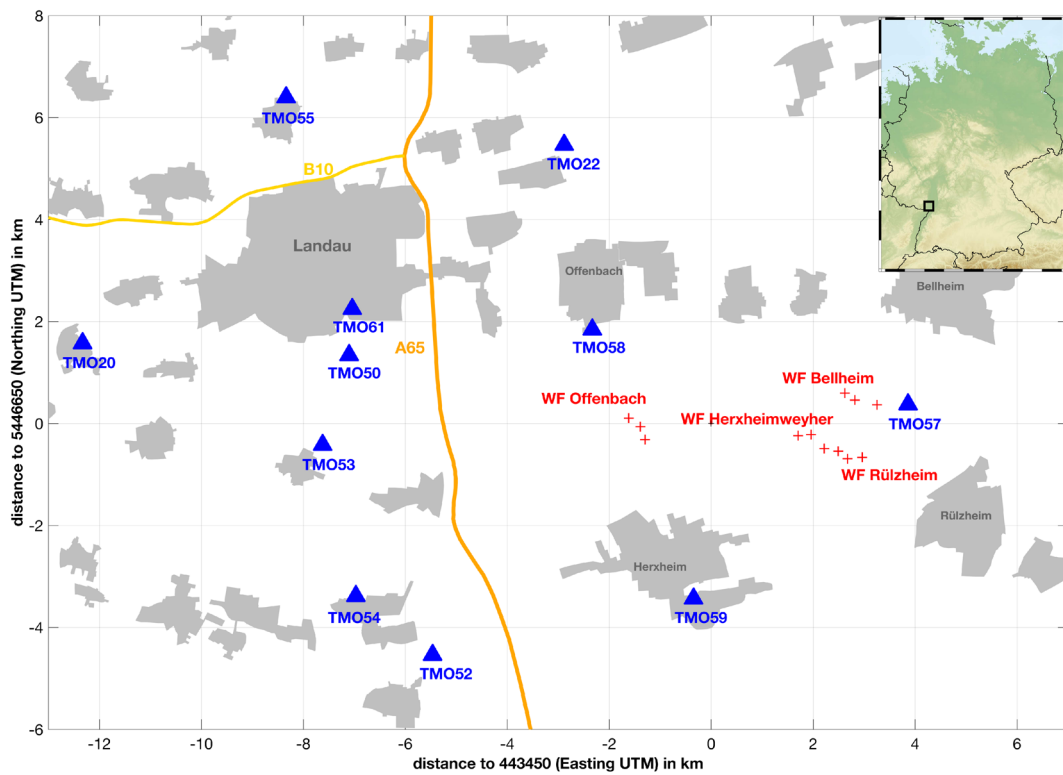

Fig. 1 Map of the study area with the seismic stations (blue triangles) used in this study, the wind turbines (red plus icons), the villages (grey), the state road B10 (yellow), and the highway A65 (orange)

3 Method and data processing

In the following section, we explain our approach to seismic interferometry and migration of source energy. All steps of data processing are implemented in MATLAB.

The seismic waveform recordings of one day (vertical component) are divided into non-overlapping time windows, whereby the length of these windows depends on the maximum distance between the seismic stations. In the current setting we use time windows with a length of 10 min (approximately six times the maximal time lag, after Groos 2010). In the next step we use a noise classification after Groos and Ritter (2009) to reject time windows containing corrupt data (e.g. due to technical problems). For most days, no time windows are excluded by the noise classification. Where time windows are rejected, their share in the total number of windows of one day is negligible ($< 2.5\%$). The cross-correlation of each seismic pair of stations is computed for a maximum time lag of 100 s. A maximum time lag of $t = S/v$ should be considered, if S is the largest inter-station distance in the network and v is a lower bound for the expected propagation velocity (we set this lower bound to 200 m/s based on the local geology). Next, a spectral whitening routine is applied to the cross-correlations for a normalization in the frequency domain. At this step, the Fourier coefficients are normalized to their maximum modulus. This routine is applied after the cross-correlation to reduce computing time. The spectral whitening leads to an enhancement of weak signals and improves the quality of our results. We stack (average) all cross-correlations of one day and apply a band-pass filter in the time domain using a 4-th order Butterworth filter to investigate signals in different specific frequency bands. The filter is applied twice (once foward and once backwards in time) to maintain the signals phase. These final, filtered stacks are the input to the migration analyses.

The stacking procedure enhances signals which appear coherent at both stations for a long time and dilutes incoherent components. We expect that the coherency of signals is due to emission by a common source. To locate these sources, we apply a migration technique which was implemented by Horstmann and Forbriger (2010) to map sources of seismic energy in the urban area of Bucharest (Romania). We illustrate the workflow of this method in Fig. 2. Signals,

continuously generated by a localized source (Q in Fig. 2) and recorded by two stations (S_k, S_l), become apparent as a transient signal in the stacked cross-correlograms at a lag time equal to the difference $\Delta t_{Q,k,l} = t_{Q,k} - t_{Q,l}$ in travel time for the two sites. We analyse data in narrow frequency bands and therefore assume a uniform propagation velocity of the observed signals. Given a hypothetical propagation velocity v (the *migration velocity*), a hypothetical source location $\mathbf{x}_Q$, and the locations $\mathbf{x}_{Sk}$ and $\mathbf{x}_{Sl}$ of stations S_k and S_l, respectively, the expected lag time is

$$\Delta t_{Q,k,l} = \frac{\left|\mathbf{x}_{Sk} - \mathbf{x}_Q\right| - \left|\mathbf{x}_{Sl} - \mathbf{x}_Q\right|}{v} \quad (1)$$

with

$$t_{Q,k} = \frac{\left|\mathbf{x}_{Sk} - \mathbf{x}_Q\right|}{v} \quad (2)$$

as the expected travel time from the source Q to station S_k. We take the envelope $E_{k,l}(t)$ of the normalized cross-correlogram for stations S_k and S_l and smooth it by applying a moving average of 2 s length (see Fig. 3 as an example). We read the value $E_{k,l}(\Delta t_{Q,k,l})$ of the envelope at the expected lag time $\Delta t_{Q,k,l}$ for the source location under consideration. The sum

$$S_Q = \sum_{k=1}^{N-1} \sum_{l=k+1}^{N} E_{k,l}(\Delta t_{Q,k,l}) \quad (3)$$

for all available pairs of the N stations is called the *semblance value*. It is a relative measure of how much signal energy a hypothetical source at location $\mathbf{x}_Q$ might have contributed to the recordings. The maximum semblance value is $S_{max} = N(N-1)/2$. If S_Q reaches this maximum value, the respective source location apparently contributes to the dominant signal in all cross-correlograms.

For the purpose of mapping, we define a grid in UTM coordinates for the area of investigation (Fig. 2) with a grid interval of 500 m. The semblance value is then computed at each grid point and interpolated in between. Because the actual propagation velocity is unknown, we repeat the mapping for a range of values for the migration velocity v. We analyse the highest semblance value in the map as a function of v. We take the value of v for the highest value of semblance as an approximation of the actual propagation velocity of the coherent signal. Typically, the highest semblance
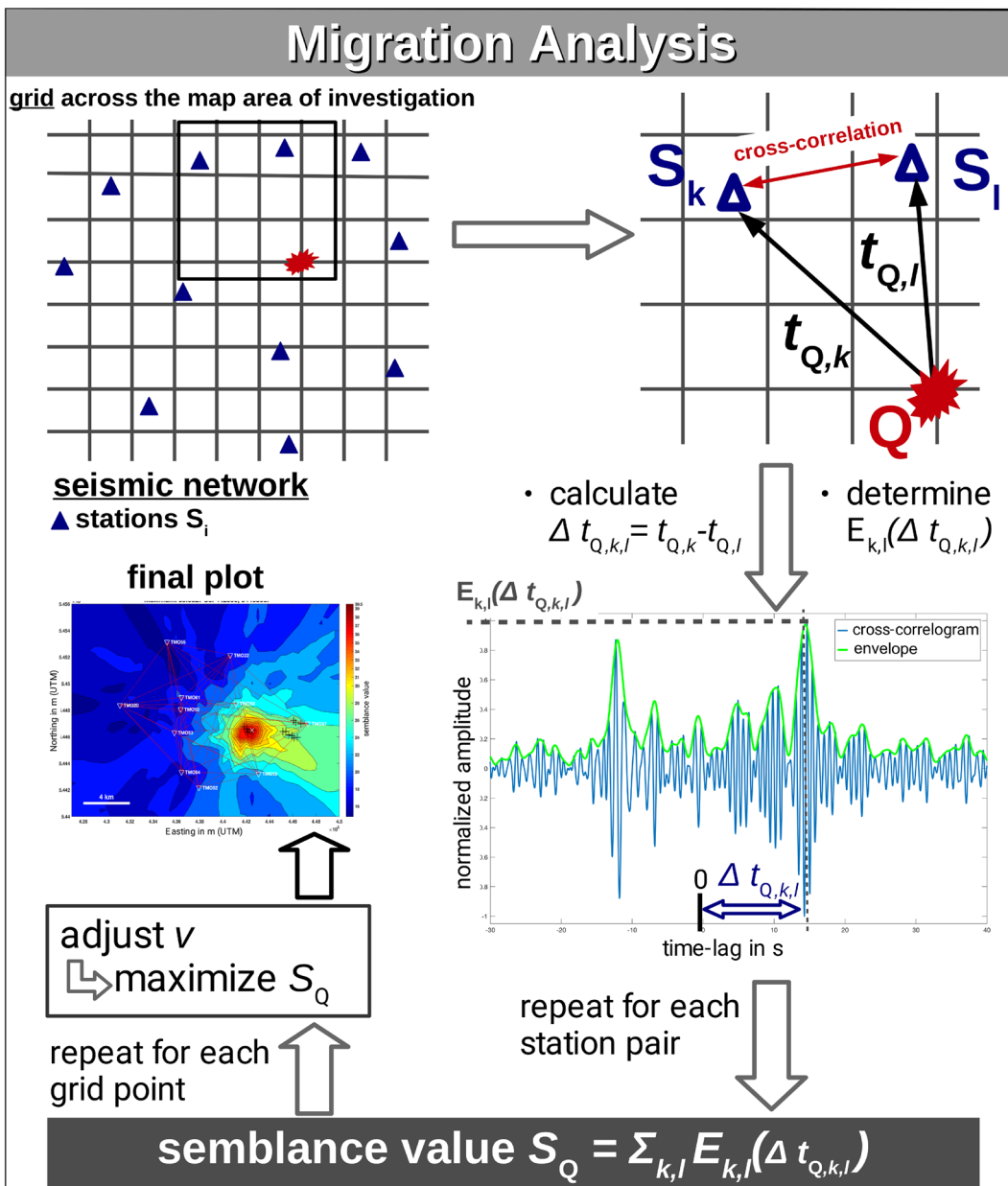
Fig. 2 Workflow of the migration analysis

values in our study appear in strongly localized spots in the area of wind farms or close to them.

4 Migration results for different frequency bands

Figure 4 shows the normalized stack of the amplitude spectra of all cross-correlations (each normalized to its maximum in the displayed frequency range)

for the 31st December 2011. Frequency bands with coherent signals are apparent through large amplitudes in Fig. 4. We focus on the bands 1.3–1.6 Hz, 1.75–1.95 Hz, and 2.0–2.2 Hz. Signals at frequencies smaller than 0.8 Hz are not relevant for our investigation. Stein (2013) showed that seismic noise signals in the range of 0.5 to 0.8 Hz are caused by a seismic source northwest of the area of investigation and that also ocean microseisms contribute to this.
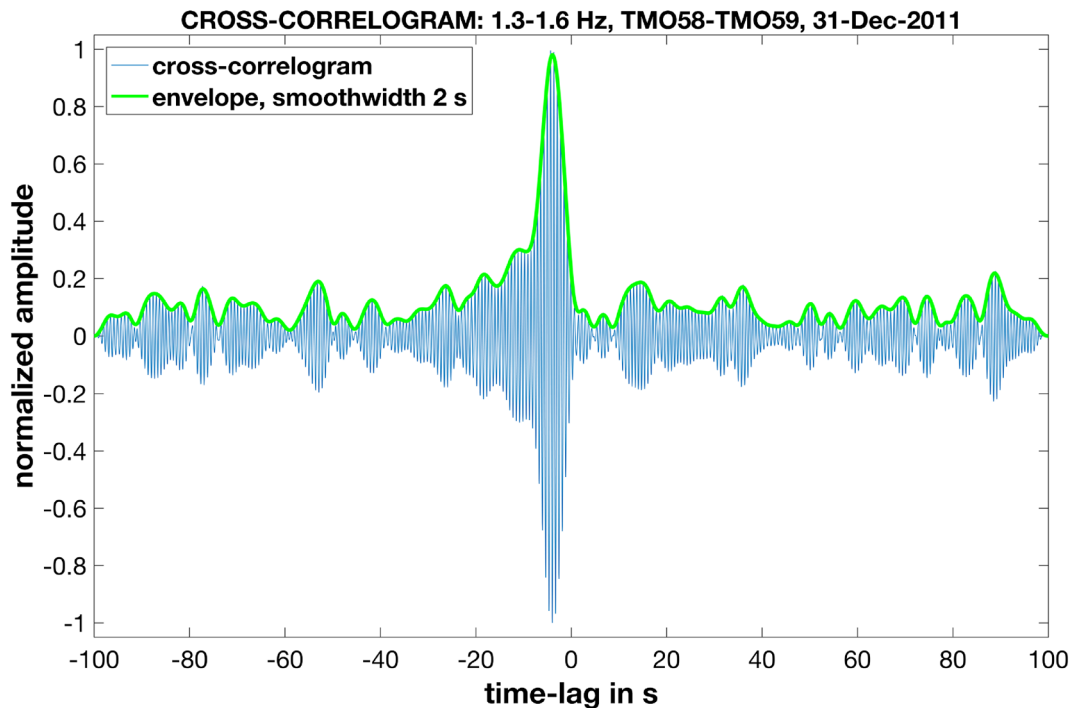
CROSS-CORRELOGRAM: 1.3-1.6 Hz, TMO58-TMO59, 31-Dec-2011

Fig. 3 Example of a cross-correlogram (normalized to its maximum) and its smoothed envelope. The maximum is located at lag time −5 s

We compute migration analyses with cross-correlation (CC) stacks of one day (*daily stack*), CC-stacks of the daily stacks of one week (*weekly stack*) or one month (*monthly stack*) in December 2011 and January 2012. These stacks are band-pass filtered for the frequency bands 1.3–1.6 Hz, 1.75–1.95 Hz, and 2.0–2.2 Hz. We tested other frequency bands as well but they lack sufficiently coherent signals.

4.1 Migration analysis for 1.3 to 1.6 Hz

In this frequency band the semblance peaks at similar locations in each of the stacks (daily, weekly and monthly). The peak semblance value varies between 43.14 and 44.93 (= 78.4 and 81.7 % of the maximum semblance value of 55). We obtain these values for a migration velocity of about 330 m/s. Figure 5 shows the result for the 31st December 2011. The mapped semblance value is specified by colour. The peak semblance value (dark red) is situated in the middle of the wind farm *Offenbach*. The three eastern wind farms *Bellheim*, *Rülzheim* and *Herxheimweyher* (see Fig. 1) are clearly marked off and apparently do not contribute to the signal. The determined location

is stable for all stacks (daily, weekly, monthly) and at least for migration velocities in the range from 300 to 350 m/s.

4.2 Migration analysis for 1.75 to 1.95 Hz

In contrast to the results in the frequency band 1.3 Hz – 1.6 Hz, the area of the peak semblance values varies stronger with the time period under investigation. Commonly, the peak location is north to northeast of the wind farm *Bellheim* and it is close to station TMO57 (about a 600 m distance to wind farm *Bellheim*). For different days and migration velocities, the source location varies by about one (easting) to two (northing) grid intervals of 500 m. We suggest that the close proximity of station TMO57 might result in some bias, though data from this station is required to provide sufficient azimuthal coverage. All remaining stations are located west of the peak location.

Figure 6 presents the results for the weekly stack from 31.12.2011 to 06.01.2012 as an example. The wind farms *Bellheim*, *Rülzheim* and *Herxheimweyher* are in the region of high semblance. They are composed of WTs with similar specifications (Table 1).
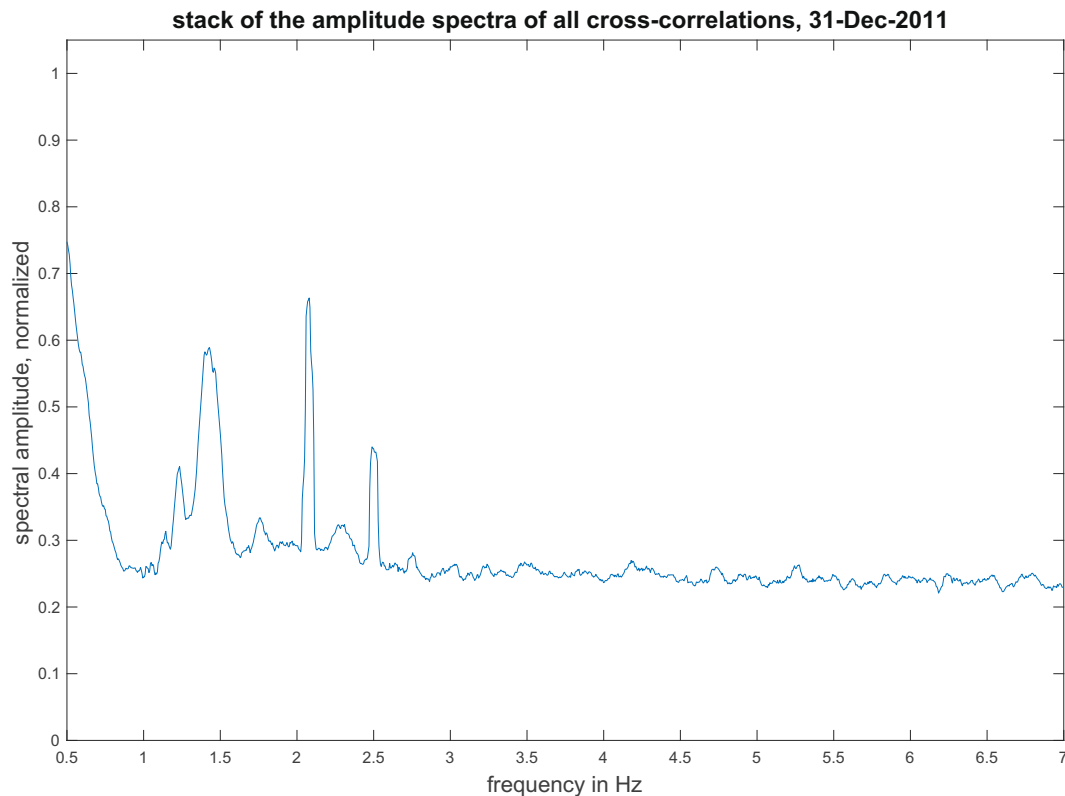
stack of the amplitude spectra of all cross-correlations, 31-Dec-2011

Fig. 4 Stack of the amplitude spectra of all cross-correlations for the 31st December 2011. Each single spectrum is normalized to one in the analysed frequency range

Therefore, we expect them to generate similar seismic signals in the frequency band from 1.75 Hz to 1.95 Hz. In this frequency band, the wind farm *Offenbach* is located in a region of distinctly lower semblance.

We obtain high peak values of semblance when using migration velocities in the range of 280 m/s to 340 m/s. The lowest peak semblance in this range is 30.66, the highest is 37.95 (55.7 % and 69.0 % of the maximum semblance value of 55, respectively). We assume that the variation in semblance value and location of the peak semblance with time and migration velocity reflects the varying contributions of the individual WTs within the three wind farms. With the available seismic data, however, we are not able to obtain the necessary spatial resolution to track this down to an individual WT. Wavelength of the analysed signals is about 150 m and hence too large to resolve individual WTs with a smaller distance within the wind farm.

4.3 Migration analysis for 2.0 to 2.2 Hz

In this frequency band, semblance typically peaks northeast of the wind farm *Bellheim*, as is displayed for the 6th January 2012 in Fig. 7. For the other analyses (daily, weekly and monthly stacks), the location of peak semblance does not differ by more than one grid interval (easting and northing). The wind farms *Rülzheim* and *Herxheimweyher* are situated in or at the boundary of the regions with high semblance values. Similar to the frequency band 1.75 to 1.95 Hz, it is likely that each WT of the three eastern wind farms emits signals in the frequency range of 2.0 to 2.2 Hz. We obtain large peak values for the semblance when using values for the migration velocity in the range of 280 to 330 m/s. Depending on the migration velocity, the location of peak semblance varies only by one grid interval in north and east direction as well. There is a large variation within the peak semblance values of about 32.77 to 41.51 (59.6 to 75.5 % of the maximum
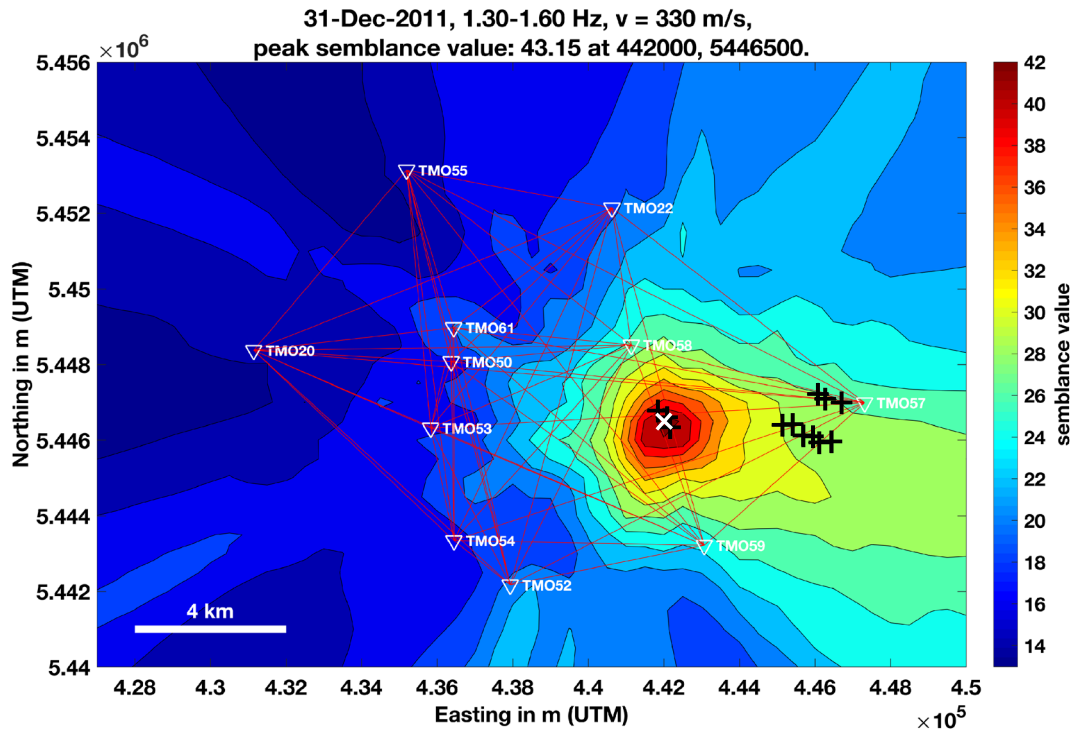
Fig. 5 Result of the migration analysis for the daily stack of the 31st December 2011 in the frequency band 1.3–1.6 Hz. The stations are marked as white reversed triangles, the wind turbines with black plus icons and the location of the peak semblance value with a white cross

semblance value of 55), comparable to the frequency band 1.75 to 1.95 Hz.

5 Dependence on wind speed

Semblance typically peaks in the vicinity of a wind farm. We take this as a confirmation that the WTs are the main source of the dominating seismic signals in the respective frequency band. A dependency on wind speed of the signal energy mapped to the peak semblance would make this statement even stronger.

The migration analysis looses this dependency when the envelope of the cross-correlogram is normalized to its maximum prior to migration. We discard this step by a modified version of the migration analysis to study the dependency of seismic energy emitted by the wind farms with data recorded in November and December 2011.

The *pfalzwind GmbH (Ludwigshafen, Germany)* provided turbine specific data such as wind speed and rotor speed of the easternmost turbine of the wind

farm *Bellheim*. Available are average values for intervals of 10 minutes measured at the nacelle height of about 100 m. We assume a sufficiently coherent wind field such that these data are valid for the whole area of investigation. We then assign the cross-correlograms of seismic recordings for the 10 minutes long time windows to wind speed classes. Table 2 specifies the range of wind speed for each wind class. The cross-correlograms are then averaged to extract coherent signal energy for each wind class. Envelopes (non-normalized) of these averaged cross-correlograms are migrated like in the previously described mapping procedure. We call the mapped value *cumulative energy* (in contrast to *semblance*), because it is proportional to the recorded wave energy due to the cross-correlation processing. It peaks at locations of strongly contributing sources and can be understood as a measure of coherent signal energy in the network. We like to point out that cumulative energy (c. e.) must not be taken as an absolute measure of seismic energy generated by a WT and we do not attribute physical units to this quantity. The
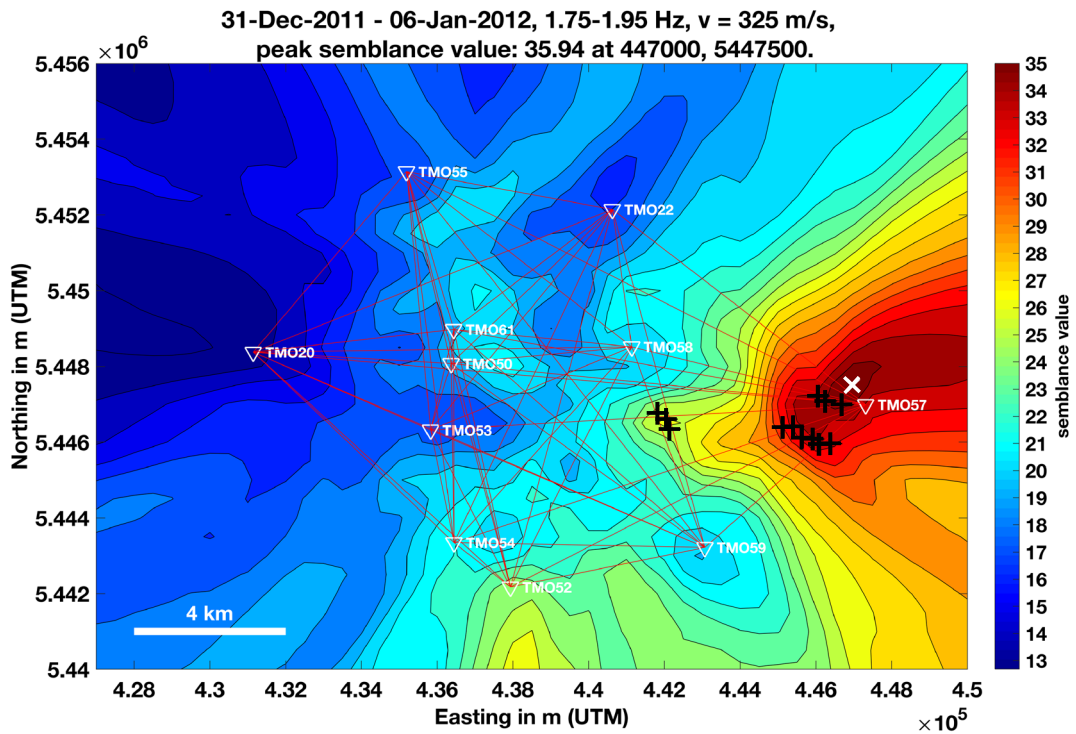
Fig. 6 Results of the migration analysis in the frequency band 1.75 Hz to 1.95 Hz: weekly stack for 31st December 2011 to 6th January 2012
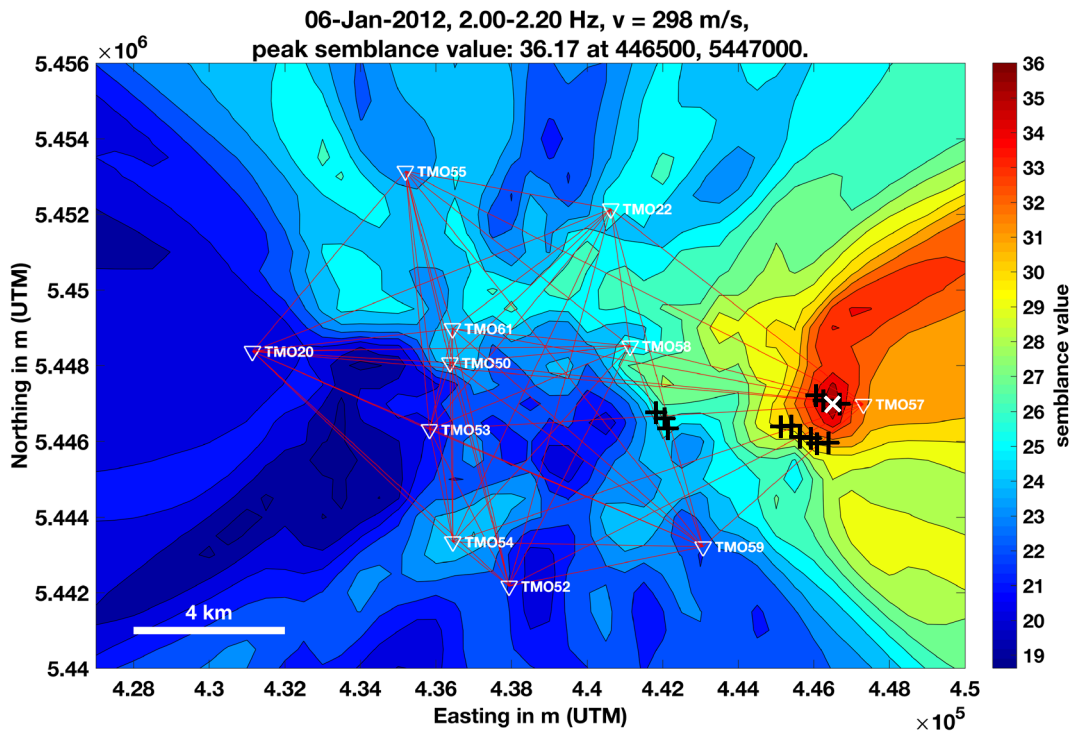

Fig. 7 Result of the migration analysis in the frequency band 2.0 to 2.2 Hz: daily stack for the 6th January 2012

Table 2 Definition of the wind speed classes depending on the wind speed v_{wind}

Wind class		1	2	3	4	5	6	7	8	9
v_{wind}	from	0	2	4	6	8	10	12	14	16
in m/s	to	2	4	6	8	10	12	14	16	18
Number of CCs		1731	1823	1527	1564	1048	643	270	76	19

The number of cross-correlations (CCs) per station pair, which are averaged at the particular wind class, is also listed

recorded signal energy decays with distance from the source and the processing does not compensate for that. Cumulative energy hence depends on the spatial configuration of the seismic network and the distance between signal source and seismic stations in particular. Equally strong signal sources can result in different peak values of cumulative energy, depending on source location. Nevertheless, a temporal variation of the cumulative energy (c. e.) mapped to the same location with an unchanged configuration of the network is a valid measure of the variation of source strength at this location. We use this property, when attributing maps of c. e. to classes of wind speed or rotor speed.

For wind class 3 and larger in the frequency bands 1.3–1.6 Hz and 1.75–1.95 Hz and for wind class 4 and larger in frequency band 2.0–2.2 Hz cumulative energy clearly peaks at the known wind farms. The locations of highest c. e. in the particular frequency bands correspond to the locations of peak semblance in Section 4. For lower wind classes (1 and 2), the peak c. e. is situated in the area of the town of Landau for all three frequency bands. Spatially secondary maxima appear for wind class 2 in the frequency band 1.3–1.6 Hz or for wind class 3 in the frequency band 2.0–2.2 Hz. At lower wind classes the emitted signals were not dominant in the area of investigation, presumably because the WTs were not producing power.

Figure 8 examplarily shows the results for the frequency range 1.3 to 1.6 Hz for wind class 2 (top) and wind class 3 (bottom). A spatially secondary maximum near the wind farm *Offenbach* can be observed for wind class 2. For wind class 3 c. e. clearly peaks at this wind farm.

The evolution of the largest value of c. e. with increasing wind class is presented in Fig. 9 for all three considered frequency bands. In this figure the c. e. is normalized to the particular maximum. The c. e. for lower wind classes is not shown due to the absence of dominating WT-induced signals in the recordings. At 1.3 to 1.6 Hz (blue line in Fig. 9) there is a distinct and nearly linearly increasing c. e. for wind classes 3 to 5. For wind classes 5 to 6, we observe a weaker increase until the value is relatively stable for wind classes 6 to 9. The reason for this behaviour presumably is a pitch of the rotor blades at a specific maximum rotor speed which is reached at wind class 6.

Signals from the wind farm *Bellheim* are dominating in the frequency band 1.75 to 1.95 Hz. In that band (green line in Fig. 9), the c. e. increases also from wind classes 3 to 6 with different slopes. The value decreases slightly from wind classes 6 to 8 and increases again from wind classes 8 to 9. It has to be mentioned that the number of averaged cross-correlations is clearly smaller for wind classes exceeding 7 and thus a statistical uncertainty must be taken into account.

In the frequency band 2.0 to 2.2 Hz (red line in Fig. 9) there is an approximately stable increase of c. e. from wind classes 4 to 7. The c. e. decreases from wind classes 7 to 8 and increases significantly from wind classes 8 to 9. Again, we like to point to the small number of cross-correlograms being available for the analysis of wind classes 7 and larger.

Figure 10 displays the rotor speed as a function of the wind speed. The operating range of the WTs starts at about 11 rpm at wind class 3. Consequently, the seismic emissions of the WTs do not dominate at wind classes 1 or 2. From wind class 6 onwards, the rotor speed is constant because the maximum permitted rotor speed of the turbine is reached. The rotor blades are adjusted (depending on the wind speed) to maintain the maximum permitted rotor speed. Due to the constant rotor speed, we expect no further increase of c. e. at wind classes larger than 6.
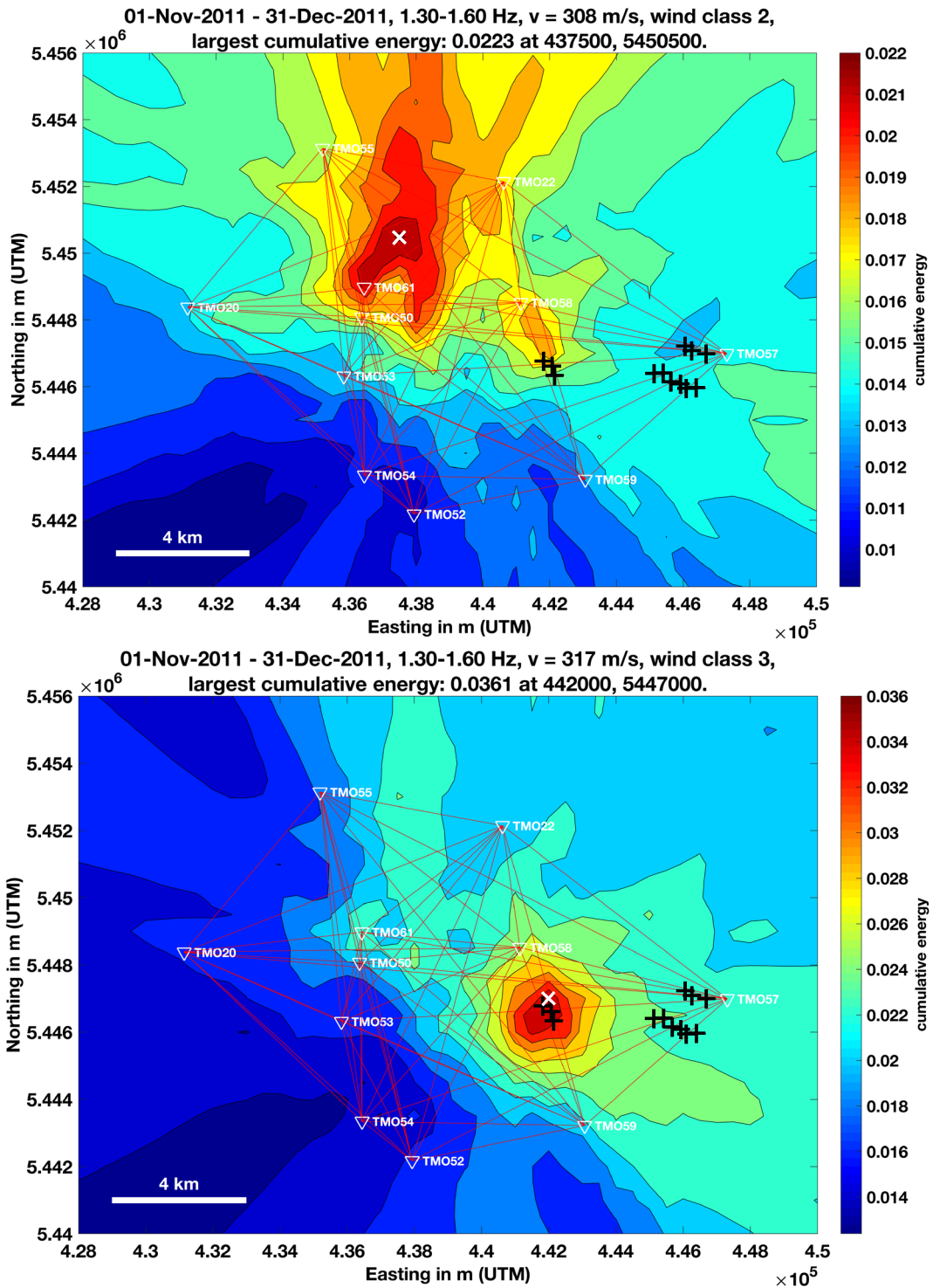
Fig. 8 Results of the migration analysis for the frequency band 1.3 to 1.6 Hz at wind class 2 (top) and wind class 3 (bottom)
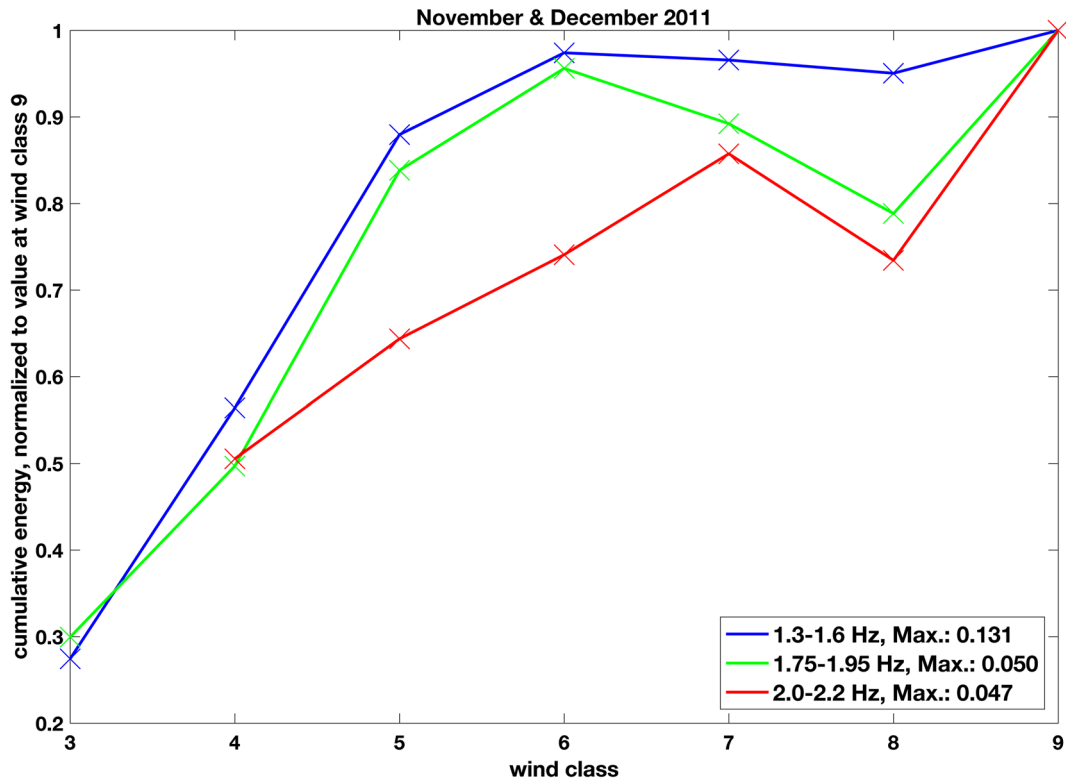
Fig. 9 Evolution of the peak cumulative energy (c. e.), normalized to the particular maximum value, with increasing wind class for the frequency bands 1.3–1.6 Hz (blue), 1.75–1.95 Hz (green) and 2.0–2.2 Hz (red). The particular maximum value of the c. e. is shown in the legend. Cumulative energy peaks at the location of wind farms when wind speed falls into wind class 3 or larger

We summarize that WT-induced signals get dominant for wind classes larger than 3 (4 to 6 m/s) or 4 (6 to 8 m/s) and that the c. e. increases clearly with increasing wind class (up to 6) respectively wind speed.

6 Mechanism of propagation of energy

Previous studies consider seismic waves as well as infrasound as possible mechanisms of propagation of energy. A major cause for vibrations in WTs are the rotor blades passing at the tower. They excite vibrations in the structure of the WT as well as pulses of air-pressure. The vibrations of the structure couple into the ground and generate seismic waves (predominantly Rayleigh waves) which propagate to the receiver. The pulses of air-pressure, however, can propagate as infrasound and couple into the ground at

a distance to the WT, such resulting in seismic ground motion too.

In the migration analysis of data recorded at Landau, semblance peaks in the vicinity of wind farms for values of migration velocity at about 320 m/s. This value is quite close to the speed of sound. Nevertheless, we believe that energy in the area of the current study predominantly propagates as seismic waves (probably Rayleigh waves).

First, a propagation velocity of 320 m/s not necessarily implies infrasound. The MAGS2 research project (Spies et al. 2017) reports values of phase velocity of 330 m/s with only weak dispersion for a frequency range of 1 to 10 Hz for the fundamental mode Rayleigh wave at different array locations near Landau. Similarly low values of shear wave velocity are also consistent with the local geology. The uppermost layers consist of loose, unconsolidated sediments which are mostly water saturated. Hence, group
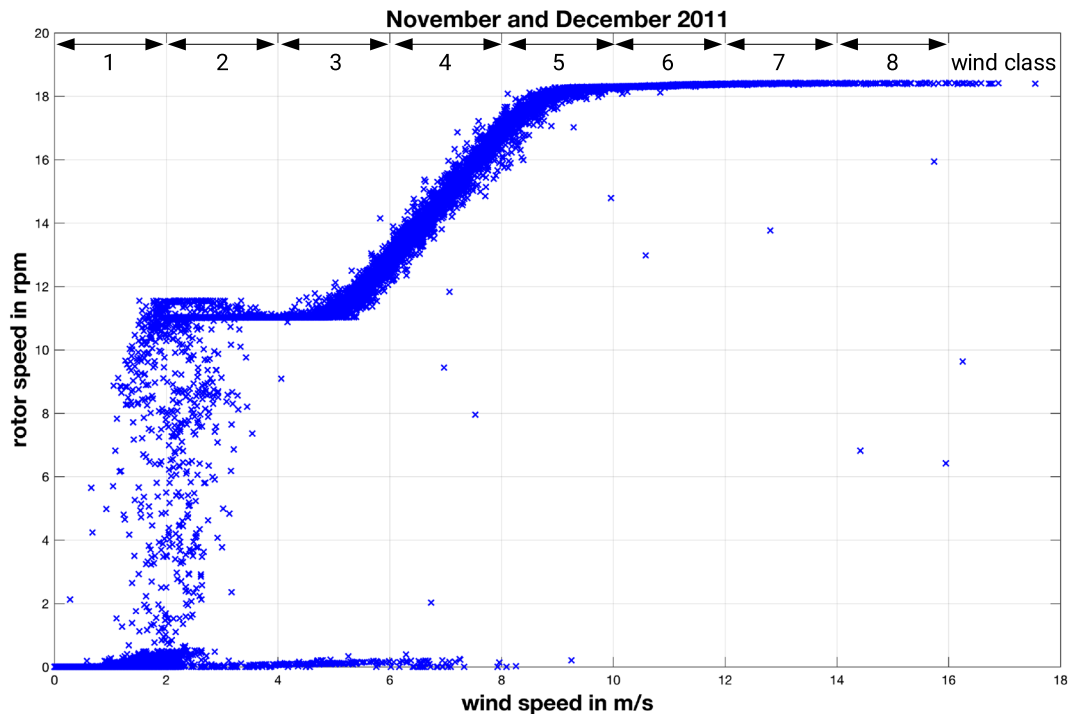
Fig. 10 Rotor speed as a function of wind speed. Measured at the easternmost turbine of the wind farm Bellheim. The wind classes are also marked

velocity of Rayleigh waves in the whole area appears to be close to the speed of sound and close to the migration velocity used in the current study.

Second, infrasound typically peaks at integer multiples of the blade-passing frequency. Pilger and Ceranna (2017, Fig. 4) resolve at least seven harmonics in a spectral analysis of infrasound pressure level, with the largest pressure signal being carried by the second harmonic. As a consequence the frequency of peaks in power spectral density depends on rotor speed and wind speed, respectively. Operational limits of rotor speed as displayed in Fig. 10 are 11 rpm at the onset of energy production at small values of wind speed and saturates at 18.5 rpm at high wind speed. The range of the first and second harmonic of the blade-passing frequency are 0.55 to 0.93 Hz and 1.1 to 1.85 Hz, respectively. We do not observe a dependency of peak-frequency in these bands on wind speed in data from Landau. In the current study and in the diagrams of power spectral density presented by Zieger and Ritter (2017, Figs. 3, 6, and 7) for the same study area peak-frequency is stable, independent of wind speed. The frequency of peaks more likely is controlled by the elastic eigenfrequencies of the resonant

structure of the towers of the WTs, which are practically constant within the resolution obtained in the analysis. This clearly indicates that vibrational energy propagates through the tower into the ground where Rayleigh waves are excited.

Thus, we suppose that WT-induced signals in the area of Landau are coupled into the ground at the foundation of the WTs and propagate as Rayleigh waves with a group velocity of about 320 m/s.

7 Summary and conclusion

By migrating the energy of cross-correlograms computed for continuous seismic signals, we locate individual wind farms as distinct sources of this energy. Wind farms (WFs) in the area under investigation are groups of three wind turbines (WTs) each. All WFs together are situated in an area extending 5 km in east-west direction and 2 km in north-south direction (Fig. 1). None of the seismic stations is positioned within this area. In a spectral analysis we observe three clear bands of spatially coherent energy at 1.3–1.6 Hz, 1.75–1.95 Hz, and 2.0–2.2 Hz which are independent

of wind speed. Seismic energy in the frequency band 1.3 to 1.6 Hz clearly originates from the WF *Offenbach* (the westernmost) with no apparent contribution by the other WFs. Signals at 2.0 to 2.2 Hz appear to be primarily generated by WF *Bellheim* (the easternmost), while WFs *Bellheim*, *Herxheimweyher*, and *Rülzheim* contribute to signals at 1.75 to 1.95 Hz. The latter three WFs are composed of WTs with the same parameters of 1.5 kW nominal power production, 100 m hub height, and 77 m rotor diameter. As demonstrated we can clearly distingiush them (through frequency band and peak location) from WF *Offenbach* which is composed of larger WTs (2.0 kW, 105 m, and 90 m).

Operating data for a WT in WF *Bellheim* is available in the current study. The range of the first and second harmonic of the blade-passing frequency in the operating range of the WT are 0.55 to 0.93 Hz and 1.1 to 1.85 Hz, respectively. The frequencies depend on rotor speed and wind speed, where both are highly correlated (Fig. 10). We do not observe this dependency of signal frequency on wind speed in seismic data. For this reason, we are convinced that the specific observed frequencies are controlled by the elastic resonance of the WTs structure. The vibrations are coupled into the ground at the foundation and probably propagate as Rayleigh waves with a group velocity of about 320 m/s.

Other than previous studies, the method proposed here enables us to study the characteristic relation between wind speed and generated seismic energy for a specific wind farm within a group of several wind farms. Migrating the observed seismic energy we are not limited to evaluate the integral seismic power of all sources. A wind farm, which presents a clear spatial peak of source energy in the migration result, can be studied independently of other WFs being present in the same study area at the same time. This way we demonstrate, that the seismic energy generated by the WTs drops to an insignificant level at values of wind speed smaller than 5 m/s. For smaller values of wind speed, source energy peaks at other locations than WFs, e.g. in an industrial area near the town of Landau. For values of wind speed higher than this threshold, continuous seismic energy in the analysed frequency bands predominantly is generated by WFs with energy level increasing with wind speed up to the upper saturation of rotor speed at about 10 m/s (Figs. 9 and 10).

References

Ballmer S, Wolfe CJ, Okubo PG, Haney MM, Thurber CH (2013) Ambient seismic noise interferometry in Hawai'i reveals long-range observability of volcanic tremor. Geophys J Int 194:512–523

Droznin DV, Shapiro NM, Droznina SY, Senyukov SL, Gordeev EIV, Chebrov N (2015) Detecting and locating volcanic tremors on the Klyuchevskoy group of volcanoes (Kamchatka) based on correlations of continuous seismic records. Geophys J Int 203:1001–1010

Flores Estrella H, Korn M, Alberts K (2017) Analysis of the influence of wind turbine noise on seismic recordings at two wind parks in Germany. J Geosci Environ Protect 5:76–91. https://doi.org/10.4236/gep.2017.55006

Gassenmeier M, Sens Schönfelder C, Delatre M, Korn M (2015) Monitoring of environmental influences on seismic velocity at the geological storage site for CO2 in Ketzin (Germany) with ambient seismic noise. Geophys J Int 200:524–533. https://doi.org/10.1093/gji/ggu413

Groos JC, Ritter JRR (2009) Time domain classification and quantification of seismic noise in an urban environment. Geophys J Int 179:1213–1231

Groos J (2010) Broadband seismic noise: classification and green's function estimation. Dissertation at the Karlsruhe Institute of Technology, KITopen ID: 1000021099. https://publikationen.bibliothek.kit.edu/1000021099

Horstmann T, Forbriger T (2010) Verbesserung einer Kreuzkorrelationsanalyse mit ungünstiger Quellverteilung durch Slant Stack und Migrationsanalyse. DGG Mittlg 2/2010:19–28. https://doi.org/10.5445/IR/1000021244

Li KL, Sgattoni G, Sadeghisorkhani H, Roberts R, Gudmundsson O (2017) A double-correlation tremor-location method. Geophys J Int 208:1231–1236

Mündel R (2009) Überwachung zeitlicher Änderungen in der Ausbreitung elastischer Wellen als Folge von CO2-Einlagerungen im Untergrund. Diplomarbeit, Institut für Geophysik und Geologie, Universität Leipzig

Neuffer T, Kremers S (2017) How wind turbines affect the performance of seismic monitoring stations and networks. Geophys J Int 211:1319–1327. https://doi.org/10.1093/gji/ggx370

Pilger C, Ceranna L (2017) The influence of periodic wind turbine noise on infrasound array measurements. J Sound Vib 388:188–200. https://doi.org/10.1016/j.jsv.2016.10.027

Ritter JRR (2011) Konzeptionelle Ansätze zur Überwachung induzierter Seismizität im Oberrheingraben in Rheinland-Pfalz. Mainzer geowiss Mitt 39:157–176

Saccorotti G, Piccinini D, Cauchie L, Fiori I (2011) Seismic noise by wind farms: a case study from the virgo gravitational wave observatory, Italy. Bull Seismol Soc Am 101(2):558–578

Schofield R (2001) Seismic measurements at the stateline wind project. Rept No LIGO T020104-00-Z, Laser Interferometer Gravitational-Wave Observatory, available at http://www.ligocaltechedu/docs/T/T01010400pdf

Sgattoni G, Gudmundsson O, Einarsson P, Federico Lucchi F, Li KL, Sadeghisorkhani H, Roberts R, Tryggvason A (2017) The 2011 unrest at Katla volcano: characterization and interpretation of the tremor sources. J Volcanol Geotherm Res 33:63–78

Shapiro NM, Ritzwoller MH, Bensen GD (2006) Source location of the 26 sec microseos, from cross-correlations of ambient seismic noise. Geophys Res Lett 33:L18310. https://doi.org/10.1029/2006GL027010

Spies T, Schlittenhardt J, Schmidt B (2017) Abschlussbericht für das Verbundprojekt MAGS2: Mikroseismische Aktivität geothermischer Systeme 2 (MAGS2) - vom Einzelsystem zur großräumigen Nutzung : Einzelprojekt EP4: Ermittlung der seismischen gefährdung bei tiefer geothermischer Energiegewinnung unter Berücksichtigung der regionalen und lokalen geologisch-tektonischen Strukturen. https://zsn.bgr.de

Stammler K, Ceranna L (2016) Influence of wind turbines on seismic records of the Gräfenberg Array. Seismol Res Lett 87(5):1075–1081. https://doi.org/10.1785/0220160049

Stein F (2013) Determination of seismic waveforms using passive seismic interferometry around Landau, SW Germany. Diploma Thesis at the Karlsruhe Institute of Technology, KITopen ID: 1000037676 https://publikationen.bibliothek.kit.edu/1000037676

Styles P, England R, Stimpson IG, Toon SM, Bowers D, Hayes M (2005) Microseismic and infrasound monitoring of low frequency noise and vibrations from windfarms: recommendations on the siting of windfarms in the vicinity of Eskdalemuir, Scotland. Keele University, UK. https://www.keele.ac.uk/geophysics/appliedseismology/wind/Final_Report.pdf

Vasterling M, Wegler U, Becker J, Bruestle A, Bischoff M (2017) Real-time envelope cross-correlation detector: application to induced seismicity in the Insheim and Landau deep geothermal reservoirs. J Seismol 21:193–208. https://doi.org/10.1007/s10950-016-9597-1

Xi Engineering Consultants Ltd (2014) Seismic vibration produced by wind turbines in the Eskdalemuir region. https://www.gov.scot/Topics/Business-Industry/Energy/Infrastructure/Energy-Consents/Guidance/reportseismicvibrations

Zeng X, Ni S (2010) A persistent localized microseismic source near the Kyushu Island, Japan. Geophys Res Lett 37:L24307. https://doi.org/10.1029/2010GL045774

Zieger T, Ritter J (2017) Influence of wind turbines on seismic stations in the upper rhine graben, SW Germany. J Seismol https://doi.org/10.1007/s10950-017-9694-9